WILEY

Neurovascular coupling in the developing neonatal brain at rest

Mina Nourhashemi | Mahdi Mahmoudzadeh [ORCID] | Sabrina Goudjil | Guy Kongolo |
Fabrice Wallois [ORCID]

INSERM U 1105, GRAMFC, Université de Picardie, CHU Sud, rue René Laennec, Amiens Cedex 1, France

Correspondence
Mahdi Mahmoudzadeh, INSERM U1105, GRAMFC, University of Picardie, CHU Sud, rue René Laennec, 80054 Amiens Cedex 1, France.
Email: mahdi.mahmoudzadeh@u-picardie.fr

Abstract

The neonatal brain is an extremely dynamic organization undergoing essential development in terms of connectivity and function. Several functional imaging investigations of the developing brain have found neurovascular coupling (NVC) patterns that contrast with those observed in adults. These discrepancies are partly due to that NVC is still developing in the neonatal brain. To characterize the vascular response to spontaneous neuronal activations, a multiscale multimodal noninvasive approach combining simultaneous electrical, hemodynamic, and metabolic recordings has been developed for preterm infants. Our results demonstrate that the immature vascular network does not adopt a unique strategy to respond to spontaneous cortical activations. NVC takes on different forms in the same preterm infant during the same recording session in response to very similar types of neural activation. This includes (a) positive stereotyped hemodynamic responses (increases in HbO, decreases in HbR together with increases in rCBF and rCMRO2), (b) negative hemodynamic responses (increases in HbR, decreases in HbO together with decreases in rCBF and rCMRO2), and (c) Increases and decreases in both HbO-HbR and rCMRO2 together with no changes in rCBF. Age-related NVC maturation is demonstrated in preterm infants, which can contribute to a better understanding/prevention of cerebral hemodynamic risks in these infants.

KEYWORDS
diffuse correlation spectroscopy, electroencephalography, near-infrared spectroscopy, premature neurovascular coupling, resting state

1 | INTRODUCTION

Dynamic interactions between the components of the neurovascular unit contribute to the complexity of brain function. There is a degree of parallelism in the co-development of neural and vascular networks, rather than separate maturation or a primary blueprint of the arrangement of blood vessels before neural elaboration/refinement. Likewise, embryonic neuronal and vascular networks may provide similar guidance cues as each system matures (Gelfand, Hong, & Gu, 2009). Neuronal and vascular networks constitute the two halves of the same functional neurovascular unit that tightly couples regional blood flow in response to local metabolic demands, known as the Neurovascular Coupling (NVC). NVC has been well characterized in adults by an increase in blood flow in response to neuronal activation (Jobsis, 1977). The balance between local consumption and arterial blood supply related to neuronal activation is much more delicate in the developing brain (Kozberg & Hillman,

2016). The way in which this NVC is affected by particular metabolic and vascular disorders (Attwell & Iadecola, 2002; Sheth et al., 2004), in the immature brain is clinically relevant with respect to the neurodevelopmental consequences of NVC dysfunction.

Functional hemodynamic imaging studies in neonates have demonstrated clearly distinct hemodynamic responses in preterm and term newborns compared to the canonical responses described in adults (Arichi et al., 2012). Data from several studies indicate that these discrepancies in hemodynamic responses might be related to the immaturity of NVC (Kozberg, Chen, DeLeo, Bouchard, & Hillman, 2013; Roche-Labarbe, Wallois, Ponchel, Kongolo, & Grebe, 2007). During the last trimester of human pregnancy, the neuronal and vascular systems both undergo major structural developments (Wallois, 2010). The processes of neuronal migration, synaptogenesis, short-range and long-range connectivity, pruning and cell death, neuronal dendritic differentiation, neurochemical maturation, and myelination gradually form the neuronal networks, providing dual innervation of pyramidal cells in preterm neonates by both subplate and thalamic axons (Arichi et al., 2010). Neural networks first undergo an active period of axonal prolongation and synaptogenesis (Lewis Jr., Courchet, & Polleux, 2013), including wiring refinement and synapse elimination (Huttenlocher, de Courten, Garey, & Van der Loos, 1982). These epochs of elaboration/refinement differ locally, but mostly progress in the human brain well into early adulthood (Harris, Reynell, & Attwell, 2011). In parallel, the vascular system undergoes a remarkable morphological development during the early neonatal period. While neurons and vasculature share guidance cues during their development (Gelfand, Hong, & Gu, 2009), gray matter perforating vessels establish rich intrinsic capillary plexuses that parallel the growth and complexity of the structurally and functionally developing cortical gray matter (Marin-Padilla, 1983). These vessels constitute the physiological locus of regulation of blood flow in response to changes in metabolic demands of local networks (Iadecola, Li, Xu, & Yang, 1996). The underlying plexus progressively differentiates into the various vascular compartments (Wang, Blocher, Spence, Rovainen, & Woolsey, 1992). This process occurs together with capillary bed expansion, remodeling, and pruning. Whether these immature neuronal and vascular networks are able to respond to metabolic demands by an increase in blood flow in preterm neonates at rest has not been fully elucidated.

Functionally, maturation of the neonatal neuronal network is associated with characteristic age-dependent transient features: (a) high-amplitude mixed frequency activities and discontinuous pattern (Wallois, 2010), reflecting the interaction between genetically encoded transient generators of the subplate and cortical plate; (b) progressively developed permanent generators and, (c) exogenous inputs from the external world (Routier et al., 2017). Some studies have suggested that spontaneous endogenous activity is critical for wiring development (Feller, 1999) by inducing neural activity that might participate in early wiring elaboration and structural and functional refinements (Ackman, Burbridge, & Crair, 2012). Discontinuous spontaneous EEG bursts of activity constitute discernible events providing an opportunity to noninvasively and passively monitor the spontaneous hemodynamic responses to endogenous

cortical activation in preterm neonates, while avoiding exogenous stimulation (Roche-Labarbe et al., 2007).

Adaptation of the immature vascular network to neuronal activation remains a subject of discussion. Animal fNIRS and fMRI studies have suggested that NVC develops postnatally (Colonnese, Phillips, Constantine-Paton, Kaila, & Jasanoff, 2007). In contrast, in preterm neonates, we observed NVC from 28 weeks GA in response to either spontaneous endogenous bursts of activity (Roche-Labarbe et al., 2007) or exogenous phonemes or voice stimulation (Mahmoudzadeh et al., 2013). Although the response of the vascular network in adults has been clearly shown to consist of positive NVC (increase in oxy-hemoglobin [HbO], total hemoglobin [HbT], and blood volume and a decrease in deoxy-hemoglobin [HbR]), increases and decreases of blood flow or blood volume have been reported in response to exogenous stimulation in neonates or preterm infants, see for example (A. P. Born et al., 2000; P. Born et al., 1998; G. Erberich, Friedlich, & Seri, 2003; S. G. Erberich et al., 2006; Heep et al., 2009; Kozberg et al., 2013; Mahmoudzadeh, Dehaene-Lambertz, & Wallois, 2017), and in immature animals (Colonnese, Phillips, Constantine-Paton, Kaila, & Jasanoff, 2007), suggesting interstudy, intersubject, and even intrasubject regional variability in early development (Kozberg & Hillman, 2016). It has also been shown that sleep influences cerebral blood flow index in neonates. The cerebral blood flow (CBF) index was lower during quiet sleep than during active sleep (Milligan, 1979; Mukhtar, Cowan, & Stothers, 1982), and higher during rapid eye movement (REM) sleep than during non-REM sleep in full-term infants (Nelle, Hoecker, & Linderkamp, 1997), while no differences in CBF were observed between active and quiet sleep, REM and non-REM sleep in preterm infants due to immaturity (Greisen, Hellstrom-Vestas, Lou, Rosen, & Svenningsen, 1985). On the other hand, the CBF index was higher during wakefulness compared to quiet sleep in preterm infants (Greisen et al., 1985). A significant hemodynamic response to burst EEG activity (increase in HbO and variable changes in HbR) has been identified in term-age infants with neurological injury (Chalia et al., 2016).

The possibility that NVC may mature in parallel with neuronal development in early infancy suggests that, during this developmental span, the neonatal brain may undergo variations in energy supply and demand dynamics in comparison to the adult brain. Coupling between hemodynamic and neuronal activity in the preterm neonatal brain at rest can be logically assumed (Roche-Labarbe et al., 2007), but whether the hemodynamic responses to bursts of activity in preterm neonates present the same patterns as in adults needs to be analyzed in more detail. Can the hemodynamic response to neural activity at rest in preterm infants be predicted in view of the complexity of the immature brain? What is the impact of various gestational ages on cerebral hemodynamic responses in the preterm neonatal brain? Is NVC age-dependent at rest? Can the neonatal cerebral cortex experience a situation of insufficient energy accessibility that alters the efficiency of cortical neurons?

To answer these questions, we will mainly focus on the coupling between spontaneous physiological bursts of activity and transient hemodynamic patterns in resting state preterm infants, in order to

more clearly characterize the underlying mechanisms that drive the coupling between the immature neuronal and cortical systems during development.

Two approaches can be considered to more clearly characterize the dynamics of the vascular network at rest in relation to spontaneous neuronal activity in preterm neonates. The first classical approach consists of considering the NVC in response to neuronal activation, that is, by analyzing the hemodynamic response to spontaneous bursts of discontinuous cortical activity in preterm neonates. The various types of hemodynamic response (directional changes in [HbO]
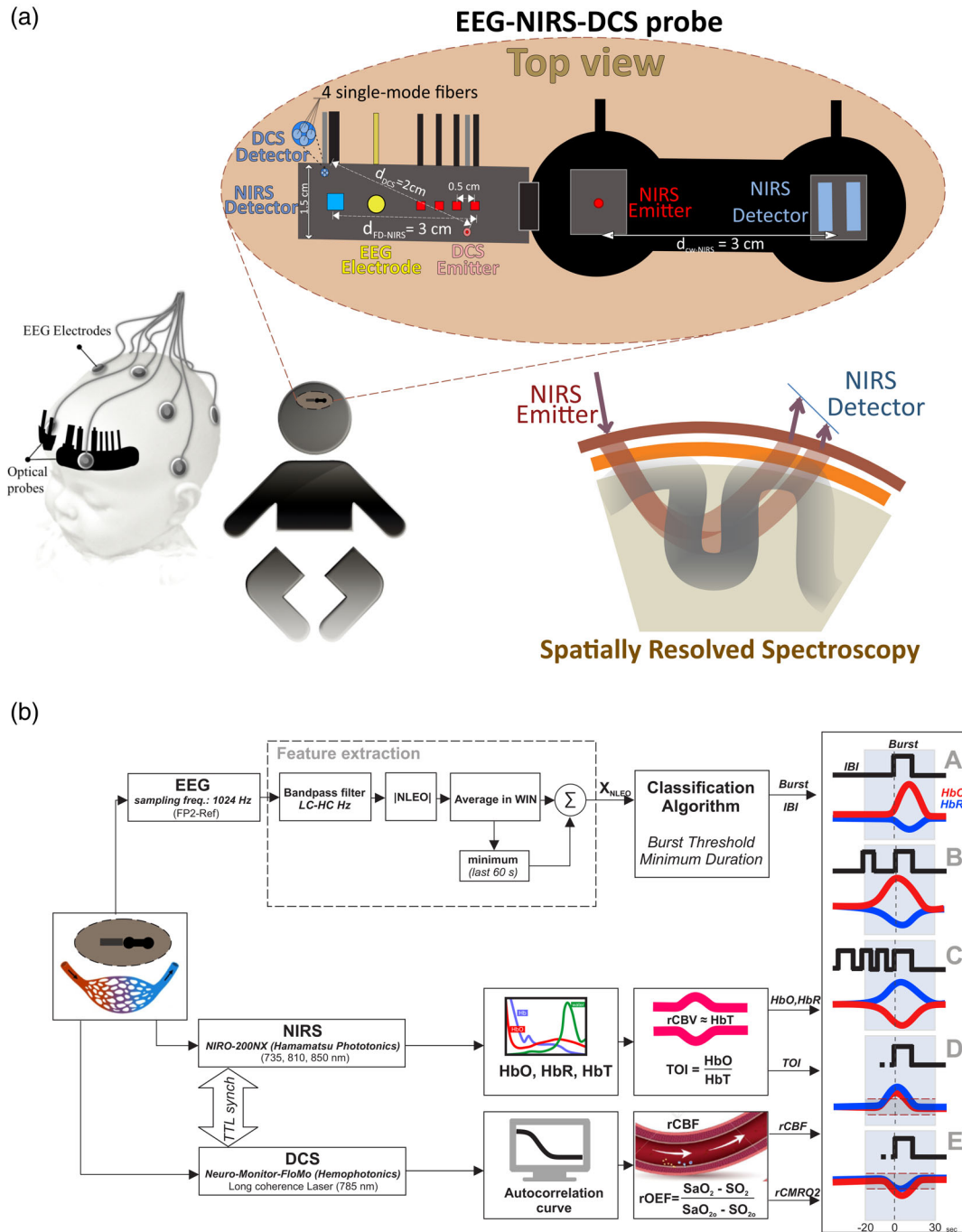
FIGURE 1 (a) Schematic representation of the location of EEG and optical probes on an infant's head. (UP) View of the hybrid optical probe constructed with a flexible hypoallergenic material and composed of three sectors: One for the DCS probe (the tips of source and detector fibers were bent to an angle of 90° and tightly held in place by rigid plastic material), one for EEG and the other for NIRS. Diagram of the frequency-domain multiple-distance (FDMD): the four emitters (red squares) are arranged on a multi-distance patch away from the detector (Gray square), creating four measurement points (channels) over the frontal area. (b) Diagram of the hemodynamic responses (HbO, HbR, calculated HbT and TOI by NIRS data, rCBF by DCS data, and calculation of rCMRO2 by NIRS data) and schematic presentation of the algorithm. |NLEO| applied on EEG signal, classification of hemodynamic responses to EEG bursts

and [HbR], cerebral blood flow and cerebral oxygenation) were analyzed by a combined simultaneous, multimodal multiscale approach using Electroencephalography (EEG) with Diffuse Correlation Spectroscopy (DCS), Continuous Wave and Frequency Domain (CW and FD) functional Near-infrared spectroscopy (fNIRS), and bedside monitoring of arterial blood pressure. The second, more recent, approach consists of considering the interaction between spontaneous oscillations of the neuronal and vascular compartments in the time-frequency domain at rest. This approach was applied to our multimodal multiscale data using a wavelet analysis method that has been shown to be suitable in neonates to provide clinical arguments to discriminate healthy neonates from asphyxiated neonates with encephalopathy (Tian, Tarumi, Liu, Zhang, & Chalak, 2016).

A hybrid EEG-NIRS-DCS patch was constructed and placed on the infant's forehead in order to perform this monitoring (Figure 1a). Eight EEG channels were recorded at the bedside in order to define the onset of the burst of spontaneous activity and quantify neuronal activation at rest. A CW near-infrared spectroscopy probe was attached in order to acquire [HbO] and [HbR] concentration changes and calculate the cerebral tissue oxygenation index (TOI). A multidistance, multichannel, frequency-domain-based optical imaging system was used to spatially assess changes in HbO and HbR at various depths and at various locations. Peripheral arterial blood pressure was monitored continuously to control systemic effects. A DCS device was connected in order to noninvasively quantify rCBF. Relative cerebral metabolic rate of oxygen (rCMRO$_2$) was estimated by using rCBF and oxygen extraction fraction (OEF). CW-NIRS continuously measures changes of HbO-HbR, while DCS and FD-NIRS are time-multiplexed (i.e., sources can be turned on and off to allow brain tissue to be illuminated for either DCS or FD-NIRS at any given time), but the tissue sampled by FD-NIRS is the same as that sampled by DCS and is closer to the EEG channel than CW-NIRS. To avoid any significant crosstalk between the CW-NIRS and FD-NIRS devices, CW-NIRS source is placed at least 5 cm apart from the DCS/FD-NIRS detector (Figure 1). The reasons to use a CW-NIRS device in addition to the FD-NIRS device were (a) The combined FD-NIRS and DCS device was necessary for CMRO2 estimation, (b) The FD-NIRS device (with multidistance source-detector probe) was used to ensure that the hemodynamic responses were not systemic, and (c) The cerebral tissue oxygenation index (TOI) measurement was performed by the CW-NIRS device (NIRO-200NX®, Hamamatsu Photonics Corp.) which is CE-approved and clinically validated system.

All data were acquired simultaneously according to a multimodal and multiscale (neuronal and hemodynamic) approach. The neuronal information provided by the EEG electrode located inside the NIRS/DCS patch was used to perform NIRS/DCS measurements as close as possible to EEG measurements. EEG and NIRS/DCS probes therefore scan identical local areas. To evaluate the effect of the burst on hemodynamic parameters, burst onset was defined as the moving average of the EEG envelope-derivative value remaining over a given threshold and was used to define time = 0 for subsequent analysis of NVC related to bursts of activity.

To extract HbO and HbR directional changes, all epochs of hemodynamic responses related to EEG bursts within the time-window [−20 to 30 s] were passed through a classification algorithm, before grand averaging. The algorithm categorizes blocks of HbO_HbR when most HbO and HbR samples are situated above or below the threshold levels of 0.05 μM or −0.05 μM after 0 s, and classifies HbO_HbR into three main conditions in the opposite direction to HbO_HbR (Condition A), in the same increasing direction as both HbO_HbR (Condition B), and in the same decreasing direction as both HbO_HbR (Condition C) (Figure 1b). Condition A was further subdivided into three subconditions according to the burst history preceding onset of the burst: (a) Subcondition A1: bursts are separated by interburst intervals (IBIs) of more than 20 s, (b) Subcondition A2: bursts are separated by IBIs of less than 20 s, including only one burst in the reference period [−20 to 0 s], (c) Subcondition A3: bursts are separated by IBIs of less than 20 s, including more than one burst in the reference period [−20 to 0 s] (Figure 1b).

The linear and nonlinear dynamics between bursts of activity and the hemodynamic response was investigated. To estimate linear interactions, we compared the root mean square (RMS) of HbO, HbR, TOI, rCBF, and rCMRO$_2$ with the RMS of the envelope derivative of the EEG bursts. The transfer entropy (TE) method based on information theory (Shannon, 1948) was used to evaluate the nonlinear interactions between EEG and NIRS changes (EEG-HbO) in preterm infants at rest, as previously described (Nourhashemi, Kongolo, Mahmoudzadeh, Goudjil, & Wallois, 2017). A new time-frequency domain wavelet analysis was applied (Tian et al., 2016) to estimate the phase and pattern of coherence between spontaneous oscillations of HbO, HbR, TOI, rCBF, and rCMRO$_2$ and the spontaneous EEG oscillations at rest, and the effect of age in the course of development in preterm neonates was evaluated.

2 | METHODS

Thirty-two preterm neonates (12 females; mean gestational age (GA) at birth: 29.3 weeks GA [27–34 weeks GA]) were tested in the supine position (recording age: 31.3 weeks GA, Table S1). This study is part of the French public hospital Clinical Research Project (PHRC National). The study was approved by the Amiens University Hospital local ethics committee according to the guidelines of the Declaration of Helsinki of 1975 (CPP Nord-Ouest II-France IDRCB-2008-A00704-51). Parents were informed about the study and provided their written informed consent.

Off-line analysis was performed using in-house MATLAB scripts for all signals. EEG artifacts were detected and rejected visually by an experienced clinical neurophysiologist (FW). A nonlinear energy operator (NLEO) algorithm was used to detect bursts of EEG activity (Vanhatalo et al., 2005). A total of 2,669 EEG bursts was detected. To provide a moving average signal, the absolute value of NLEO output was then smoothed by calculating the average in a 1.5-s sliding window. Artifacts (mostly due to movement), observed in both the EEG and optical signals, were removed from both signals. A z-score-based
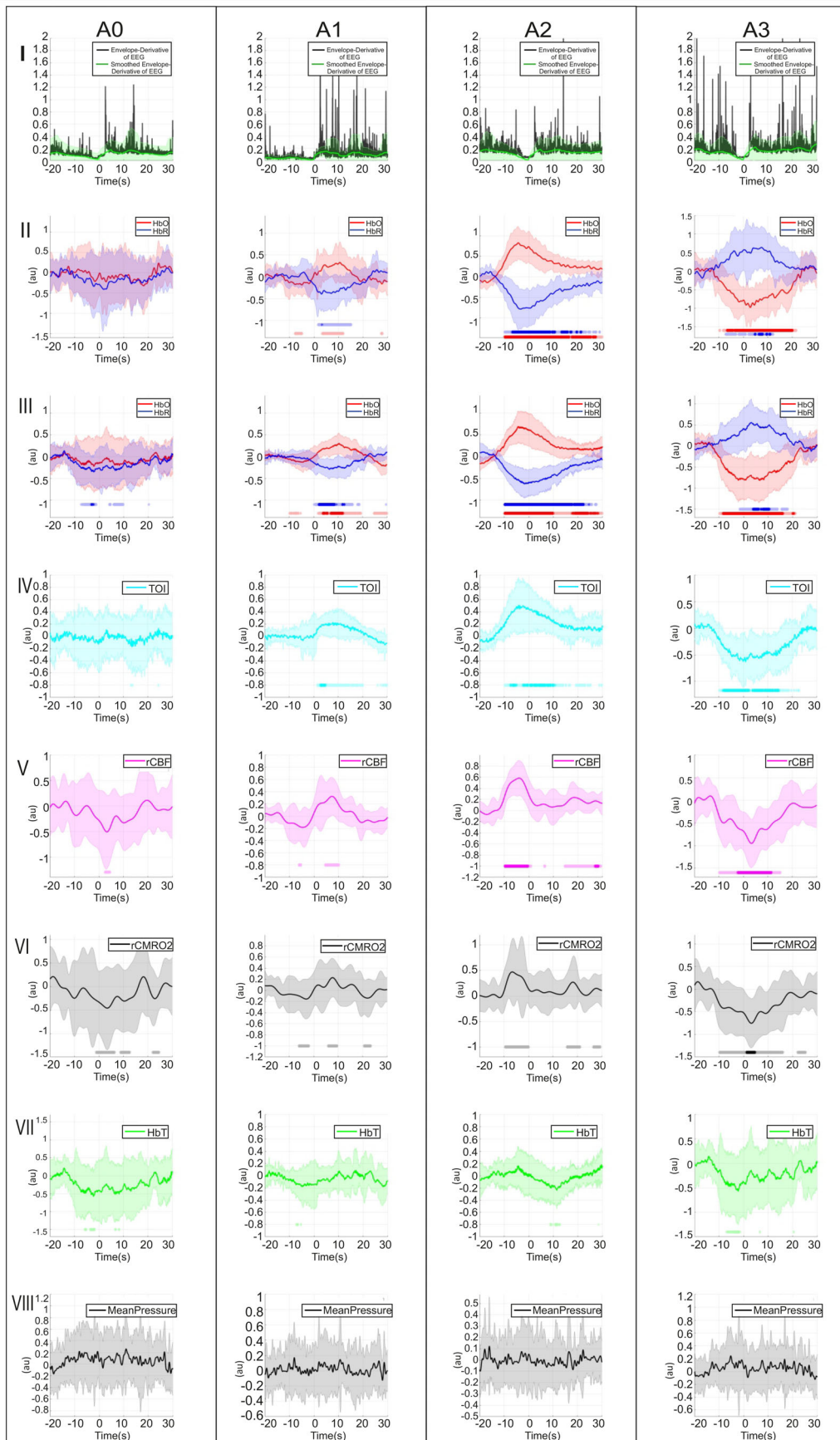
FIGURE 2   Legend on next page.

algorithm was used to reject artifacts from optical signals (A. P. Born et al., 2000). The remaining cleaned hemodynamic signals were band-pass filtered [0.03–0.5 Hz] to eliminate physiologic noise. The hemodynamic responses (HbO, HbR, TOI, rCBF, rCMRO$_2$, and HbT [as a surrogate measurement of CBV]) time-locked to the EEG signal were averaged (time window: [−20 to 30 s]).

In a first step, all trials of hemodynamic responses related to EEG bursts were averaged regardless of the IBI: Subondition A0 (Figure 2, A0). In a second step, all trials of hemodynamic responses related to EEG bursts were submitted to a classification algorithm and classified into three main conditions according to the IBI and the number of bursts (0, 1, or 1+ bursts) occurring during the reference period [−20 to 0 s].

- Condition A: The hemodynamic response is evaluated with 0, 1, or 1+ bursts occurring during the reference period.
  - Subcondition A1: bursts are separated by IBIs longer than 20 s (Figure 2, A1), meaning that no burst of activity was observed during the reference period [−20 to 0 s].
  - Subcondition A2: bursts are separated by IBIs shorter than 20 s, including only one burst in the reference period [−20 to 0 s], (Figure 2, A2).
  - Subcondition A3: bursts are separated by IBIs shorter than 20 s, including more than one burst in the reference period [−20 to 0 s], (Figure 2, A3).

In the last step, all trials of hemodynamic responses related to EEG bursts were passed through the hemodynamic response classifier to take into account the possibility that the hemodynamic response might be characterized not only by a canonical NVC (opposite changes in HbO and HbR), but also by changes of HbO and HbR in the same direction, resulting in a change in cerebral blood volume (CBV) without no changes in cerebral blood flow (CBF):

- Condition B: The hemodynamic response consists of opposite changes in HbO and HbR.
  - Subcondition B1: bursts are separated by IBIs longer than 20 s (Figure 3, B1).
  - Subcondition B2: bursts are separated by IBIs shorter than 20 s, including only one burst in the reference period [−20 to 0 s] (Figure 3, B2).
  - Subcondition B3: bursts are separated by IBIs shorter than 20 s, including more than one burst in the reference period [−20 to 0 s] (Figure 3, B3).

- Condition C: The hemodynamic response consists of similar changes in HbO and HbR.
  - Subcondition C1: The hemodynamic response consists of an increase in HbO and HbR (Figure 3, C1).
  - Subcondition C2: The hemodynamic response consists of a decrease in HbO and HbR (Figure 3, C2).

In order to compare the hemodynamic responses in the various conditions, statistical analyses (Student's t test) were performed on the amplitude of the hemodynamic signals in the different subconditions (A1, A2, A3). Also, in order to take into consideration that the variations of the two sets of responses (positive vs. negative NVC) were recorded within the same subject, a paired sample t test (degree of freedom: 31) was applied using SPSS® software. In a first step; a paired sample t test was applied between the two groups (positive NVC conditions A1, A2 vs. negative NVC Condition A3) to compare the number of hemodynamic responses. In a second step; to take into consideration the opposite directions of HbO and HbR responses such as in a typical positive or negative NVC, we calculated the mean value of Hb difference (HbD) index [HbD = oxyhemoglobin (HbO) − HbR]; for each subject in each condition (A1, A2, and A3) between 0 and 20 s. Since the hemodynamic patterns were identical in A1 and A2 conditions, their indices were pooled and compared to A3 condition. To compare this HbD index in negative and positive NVC, a paired sample t test was applied between two groups: Positive (Conditions A1, A2) versus Negative NVC (Condition A3; see Tables S3 and S4 for more details).

2.1 | Wavelet coherence analysis of NVC

To estimate the cross-correlation between spontaneous oscillations in hemodynamic signals and spontaneous EEG at the resting state, a new time-frequency domain wavelet analysis was applied (Grinsted, Moore, & Jevrejeva, 2004). The statistical significance level of R^2 (squared wavelet coherence) can be assessed based on a Monte Carlo simulation of a stochastic Gaussian process (Maraun & Kurths, 2004). The percentage of significant coherence was further calculated as a function of age.

2.2 | Linear and nonlinear EEG_hemodynamic response interactions

The linear correlation between RMS of EEG and RMS of hemodynamic responses and the nonlinear relationship between EEG and hemodynamic signals (NIRS, DCS data) by using transfer entropy (TE) were

FIGURE 2 The grand average of the regional hemodynamic responses of the onset of EEG bursts at 0 s (the time duration is shown 20 s before and 30 s after the onset of the EEG burst, and the first 10 s was defined as baseline). The longitudinal panels indicate envelope-derivative of EEG and moving average of envelope-derivative over all EEG bursts in one subject (I), the grand average of changes in HbO_HbR measured by ISS (II), the grand average of changes in HbO_HbR measured by Hamamatsu (III), the grand average of changes in TOI (IV), rCBF (V), and rCMRO$_2$ (VI). The vertical panels related to the classification of the bursts of activity, the grand average of all the Bursts (whatever the IBI; A0), with no EEG burst during the previous 20 s (A1), one EEG burst during the first 20 s (A2), two or more EEG bursts during the first 20 s (A3). The annotations below the signal highlighting the durations of hemodynamic responses were significantly different from the reference period (−20 to −10 s), light stars related to (t test, $p < .001$) and dark stars related to (t test, $p < 1.1e−6$). Shaded error bars indicate the standard deviations for the corresponding signals at each time-point
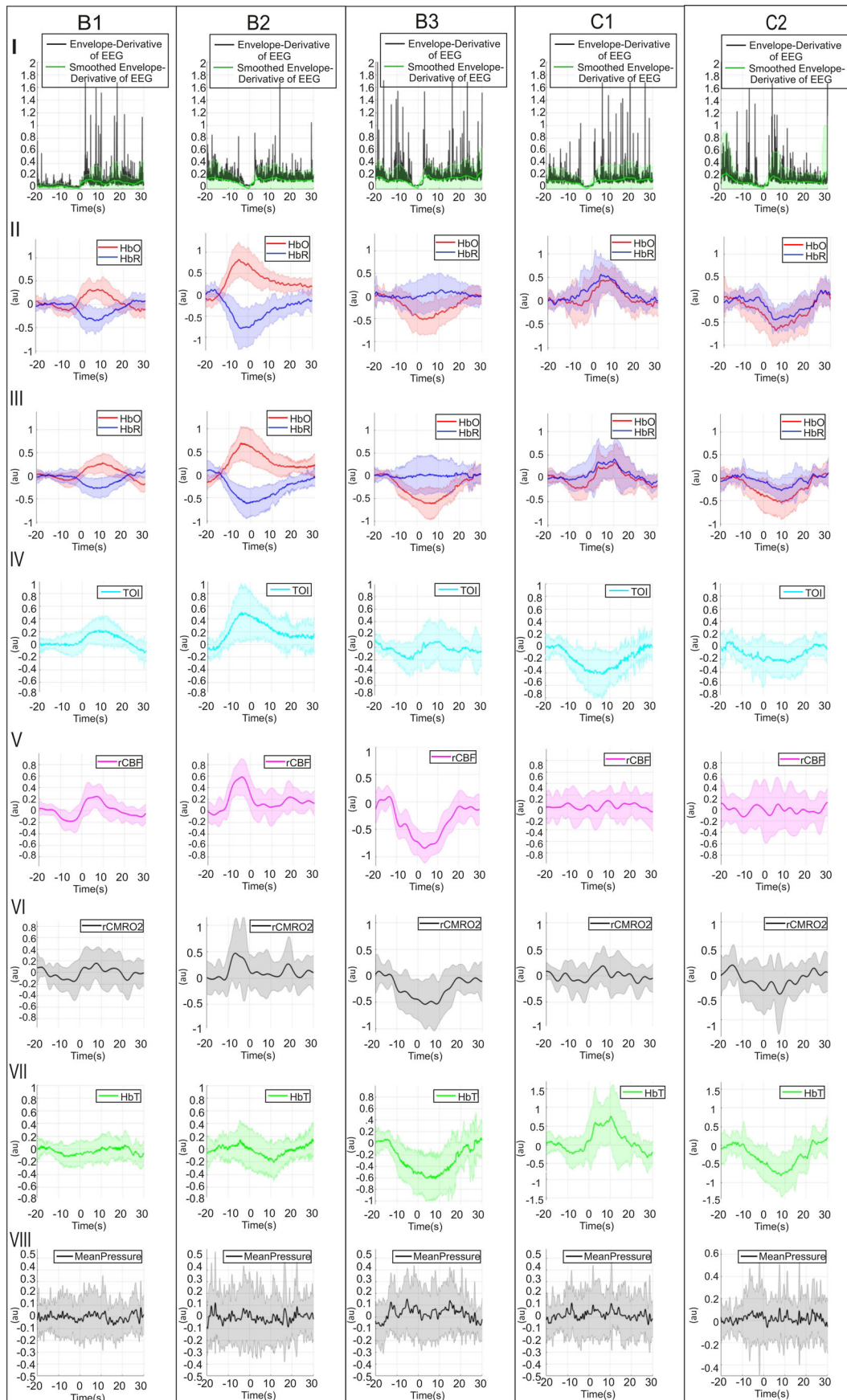
FIGURE 3 Legend on next page.

investigated. Statistical analysis was performed according to the surrogate method (Nourhashemi et al., 2017).

For more details, please see the Supporting Information.

3 | RESULTS

Discontinuous bursts of EEG activity were first detected by the NLEO algorithm (Vanhatalo et al., 2005) and were then validated by an experienced neurophysiologist (FW). The percentages of classified hemodynamic responses to EEG bursts in each condition, with no significant changes, are presented in Table S2.

3.1 | Cerebral hemodynamic responses to bursts of activity in normal preterm neonates

The grand average of the changes of the various hemodynamic parameters were calculated (HbO-HbR, TOI, and rCBF) and estimated (rCMRO$_2$) relative to the onset of the detected burst of activity after grand averaging of the envelope derivative of the EEG and a moving average of this envelope over all bursts (Figures 2 and 3).

3.2 | Hemodynamic response to all bursts without considering the IBIs

This condition corresponds to Subcondition A0 in Figure 2. No significant changes were observed in [HbO], [HbR], [HbT], TOI, rCBF, CBV, and rCMRO2.

3.3 | Hemodynamic response to all bursts, taking into account the IBIs

The hemodynamic responses were observed in Condition A, during which the rCBF hemodynamic response consisted of opposite changes in HbO and HbR. Subconditions A1 and A2 were also more frequent with positive NVC and an increase in rCBF. In Subcondition A1, the bursts were separated by IBI lasting more than 20 s (Figure 2, A1). In this subcondition (A1), hemodynamic changes started well before onset of the burst and consisted of an initial decrease in HbO starting −12.5 s before the onset of the burst (t0), which was significant ($p < .001$) between −7.8 and −4.7 s, followed by an increase in HbO starting −0.5 s before t0, which was significant ($p < .001$) between 3.2 and 12 s. The subsequent increase was concomitant to the burst of activity (Figure 2, A1-II). A slight, nonsignificant increase in HbR was

followed by a decrease in HbR starting −3 s before t0, which was significant ($p < .001$) from −1.6 to 15.3 s (Figure 2, A1-II). The increase in TOI also started before onset of the burst (−0.1 s), but was only significant ($p < .001$) from 1.3 to 20.2 s (Figure 2, A1-IV). The decrease in regional rCBF (and rCMRO$_2$) also started before the onset of the burst (−13.1 and −15 s, respectively) and was significant ($p < .001$) from −6.2 to −5.1 s and again from 4.3 to 10.2 s for rCBF and from −6.2 to −1.8 s and 5.8 to 9.6 s for rCMRO$_2$. rCBF (rCMRO$_2$) then started to increase at the onset (t0) of the EEG burst (Figure 2, A1-V–VI). rCBF and rCMRO$_2$ returned to baseline more rapidly than HbO_HbR. The decrease in CBV (HbT) started before onset of the burst (−13 s) and was significant ($p < .001$) from −7.3 to −5.3 s. No significant changes in CBV were observed (Figure 2, A1-VII). Subconditions A2 and A3 were considered in order to evaluate the impact of the previous bursts on the hemodynamic responses. In Subcondition A2, the bursts were separated by IBIs lasting less than 20 s and only one burst occurred in the reference period [−20 to 0 s] (Figure 2, A2). In Subcondition A2, as in Subcondition A1, the hemodynamic response started with a significant increase ($p < .001$) in HbO, TOI, rCBF, rCMRO$_2$ and a significant decrease ($p < .001$) in HbR beginning −10 s, before onset of the burst (Figure 2, A2). The amplitude of the hemodynamic response was significantly higher ($p < .05$) than in Subcondition A1 (Figure 2, A2 vs. A1). No significant changes in CBV were observed (Figure 2, A2-VII). In Subcondition A3, the bursts were also separated by IBIs lasting less than 20 s, but more than one burst occurred in the reference period [−20 to 0 s] (Figure 2, A3). Compared to the previous Subconditions A1 and A2, the hemodynamic response was completely inverted, consisting of a significant decrease ($p < .001$) in HbO, TOI, rCBF, rCMRO$_2$ and a simultaneous significant increase ($p < .001$) in HbR, starting −10 s before onset of the burst. A significant decrease in CBV was observed in relation to the burst of activity (Figure 2, A3-VII).

3.4 | Hemodynamic response to all bursts, taking into account the IBIs and the possibility of changes in HbO and HbR in the same direction

Four types of responses were observed: (a) a rCBF response with either a positive or negative change in rCBF (Subconditions B1, B2, and B3) or (b) a CBV response with either a positive or negative change in CBV (Subconditions C1 and C2).

In Condition B (Subconditions B1, B2, and B3), the changes in the hemodynamic responses were similar to those observed in Condition

FIGURE 3 The grand average of the regional hemodynamic responses of the onset of EEG bursts at 0 s (the time duration is shown 20 s before and 30 s after the onset of the EEG burst, and the first 10 s was defined as baseline). The longitudinal panels indicate envelope-derivative of EEG and moving average of envelope-derivative over all EEG bursts in one subject (I), the grand average of changes in HbO_HbR measured by ISS (II), the grand average of changes in HbO_HbR measured by Hamamatsu (III), the grand average of changes in TOI (IV), rCBF (V), and rCMRO$_2$ (VI). The vertical panels related to the classification of the bursts of activity, with no EEG burst during the previous 20 s (B1), one EEG burst during the first 20 s (B2), two or more EEG bursts during the first 20 s (B3) and the vertical panels (C1 and C2) related to the bursts of activity that accompany the increase in both HbO_HbR (C1) and the decrease in both HbO_HbR (C2). Shaded error bars indicate the standard deviations for the corresponding signals at each time-point

A (Subconditions A1, A2, and A3), but the amplitude of the hemody-namic responses was more pronounced for all parameters (Figure 3b). In Condition C (Subconditions C1 and C2), the hemodynamic responses were very different and were mainly characterized by changes in CBV. Although the difference between Figure 2 and Figure 3 is based on the use of a different classification, the differ-ence between Subconditions (A1, A3) and Subconditions (B1, B3) is likely due to the separation of hemodynamic patterns into

Subconditions C1 and C2 from Subconditions (B1, B3), since most patterns in Subconditions C1 and C2 are related to EEG bursts, including more than one (sometimes including zero) EEG burst during the reference period.

In Subcondition C1, the responses consisted of a simultaneous increase in both HbO and HbR and $rCMRO_2$ with no changes in rCBF and TOI (Figure 3, C1). In contrast with the previous Condition B, CBV increased during the burst of activity (Figure 3, C1-VII).
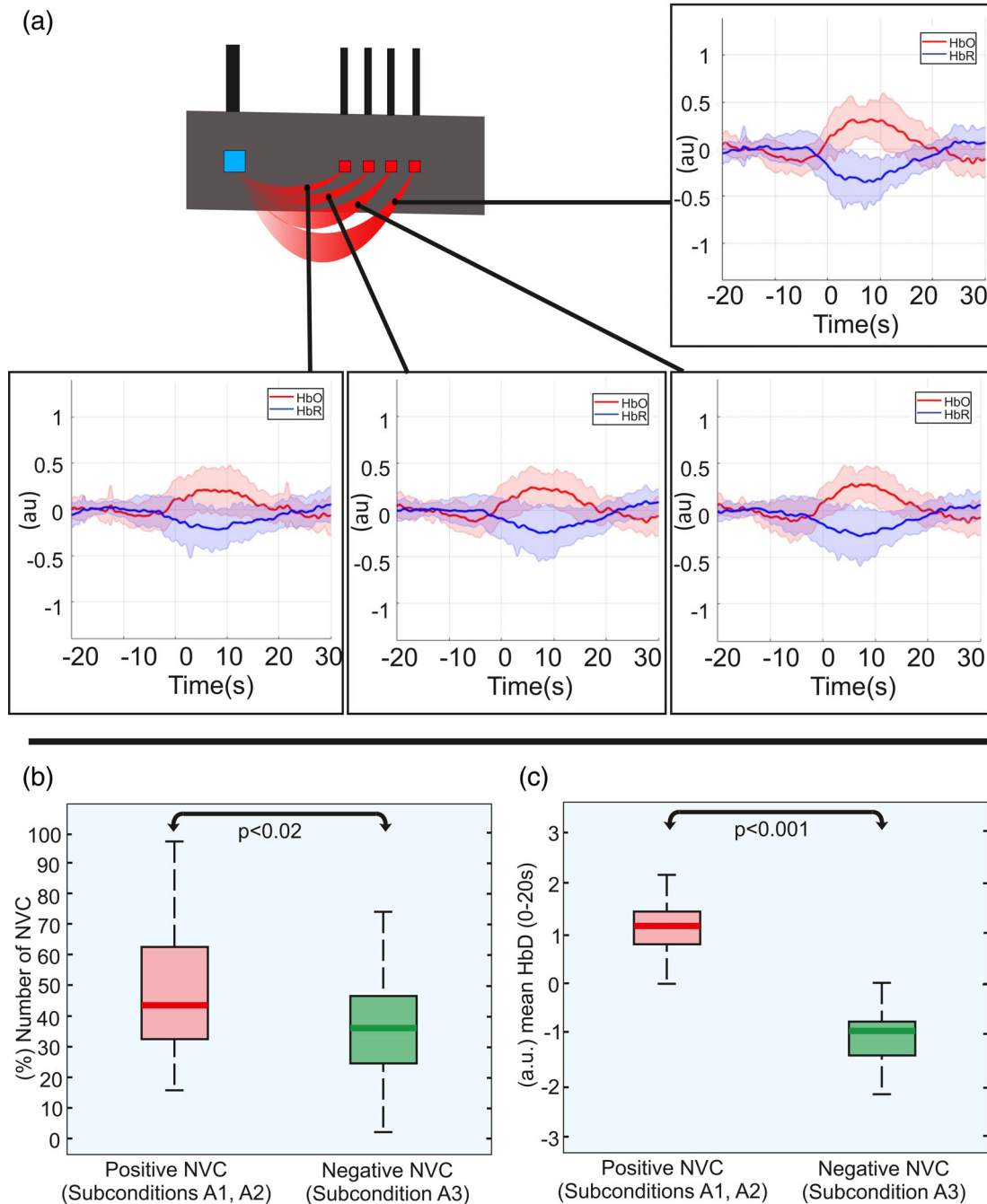
FIGURE 4 (a) The grand average of changes in HbO_HbR measured with multidistance NIRS (ISS). (b) Comparing the number of hemodynamic responses between Positive NVC (Conditions A1, A2) versus Negative NVC (Condition A3) using a paired sample t-test. (c) Comparing the HbD (0–20 s) mean values between Positive NVC (Conditions A1, A2) versus Negative NVC (Condition A3) using a paired sample *t* test

In Subcondition C2, the hemodynamic response was opposite to that observed in Subcondition C1, but the CBV effect remained the dominant effect. The responses consisted of decreases in HbO, HbR, TOI, and rCMRO$_2$, with no changes in rCBF (Figure 3, C2), resulting in a

decrease in CBV during the burst of activity (Figure 3, C2-VII). Similar dynamics of HbO and HbR fluctuations were observed whether frequency-domain fNIRS or continuous-wave fNIRS was used (Figure 3, II and III) and regardless of the distance between emitters
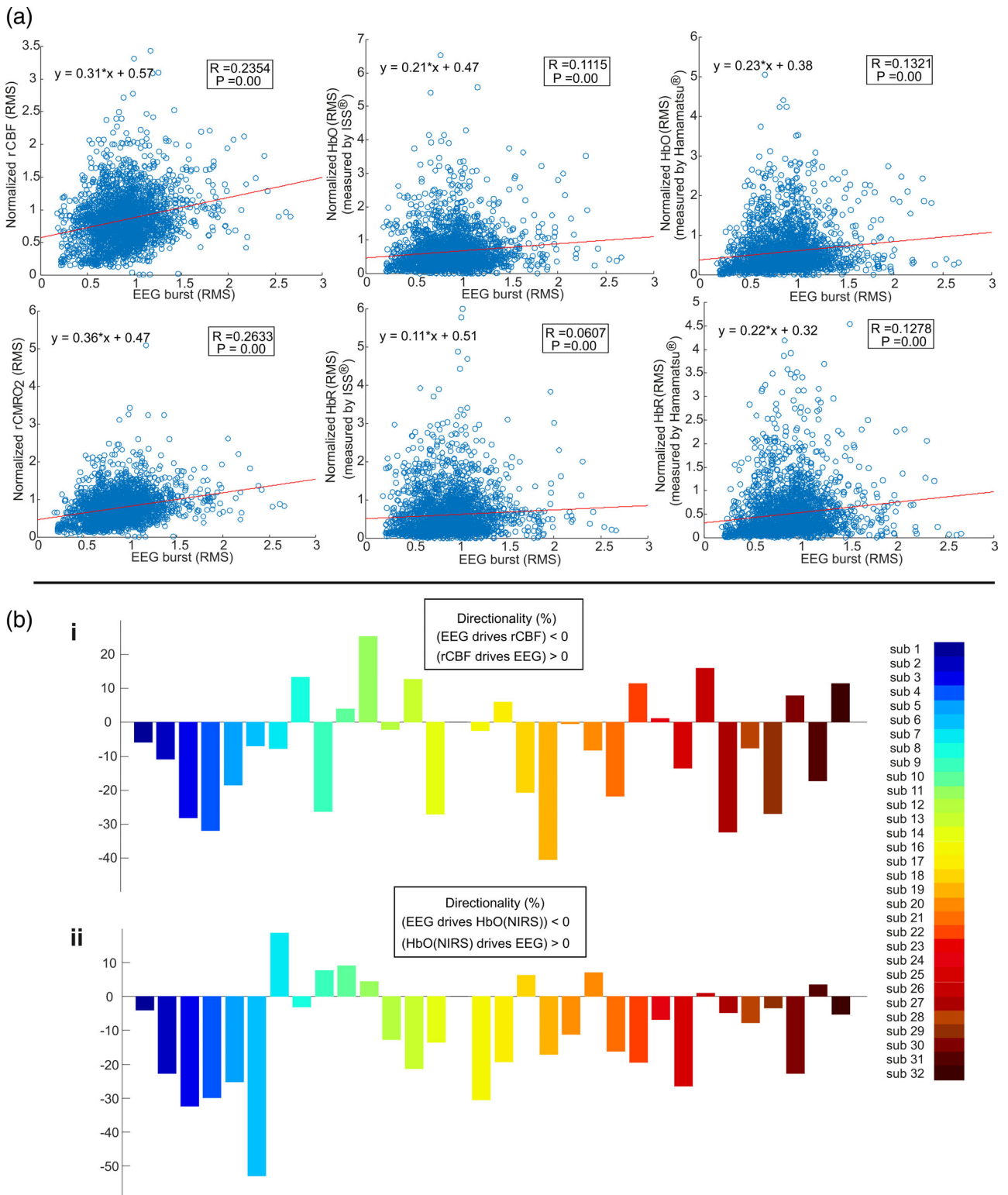
FIGURE 5 (a) Correlation between RMS of hemodynamic responses and RMS of EEG bursts. (b) Rate of information (TE) exchanged from RMS-EEG to CBF (RMS-EEG to HbO) (i), and vice versa (ii)

and detectors of two devices. In addition, these bursts of activity did not induce any systemic changes in arterial blood pressure (ABP; Figure 3, VIII).

Figure 4a shows the changes in HbO-HbR for different distances between emitters and detector. The most prominent hemodynamic changes were observed for a longer distance, suggesting that these
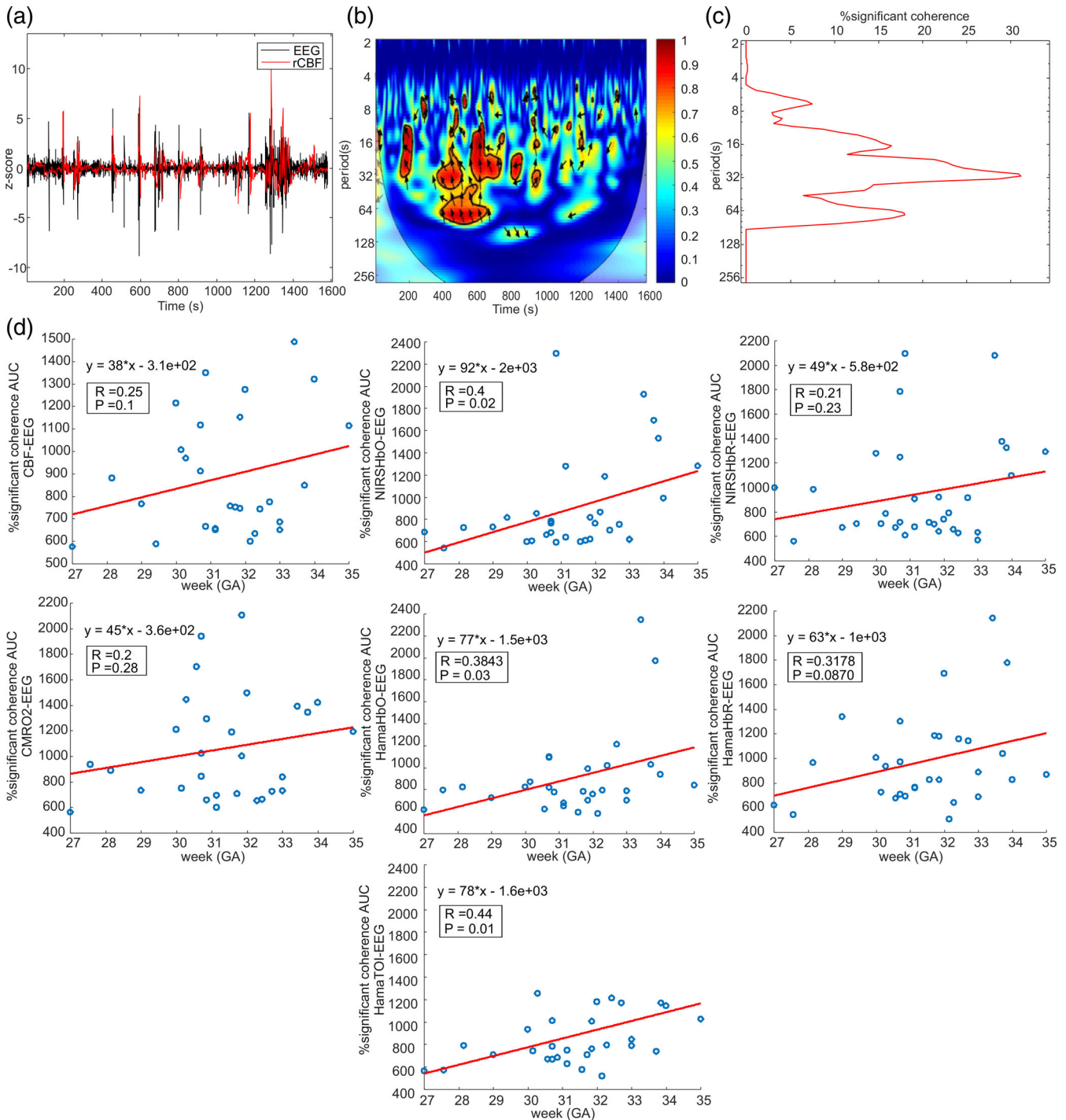
FIGURE 6 (a) An enlarged segment of real-time rCBF and EEG data from a sample of healthy preterm neonate #32. Quantification of results by wavelet coherence analysis: (b) Squared cross-wavelet coherence, $R_{CBF \rightarrow EEG}$. The x-axis represents time, the y-axis represents scale (which has been converted to the equivalent Fourier period), and the color scale represents the magnitude of R^2. The black line contours designate areas of significant coherence ($p < .05$). The arrows designate the relative phase between rCBF and EEG: a rightward-pointing arrow indicates in-phase coherence between the two signals ($\Delta\varphi = 0$), a leftward-pointing arrow indicates anti-phase coherence ($\Delta\varphi = \pi$). (c) Percentage of significant coherence is quantified in each of the two phase ranges as a function of scale, which is plotted on the y-axis (that has been converted to equivalent Fourier period). (d) The percentage area with high NVC coherence over the total area considered for each preterm neonate as a function of age

changes are more pronounced in deeper layers and therefore reflect the cortical origin of the hemodynamic changes. Only the changes related to the longer distance are therefore reported and analyzed (Figure 2, II and Figure 3, II).

The number of hemodynamic responses to EEG bursts was compared between two groups: positive NVC (Subconditions A1, A2) versus negative NVC (Subcondition A3). Figure 4b shows a significant difference between the number of positive versus negative NVC (paired sample t test, $p < .02$). Also, the mean HbD (oxyhemoglobin (HbO) − HbR) from 0 to 20 s was compared between positive (Conditions A1, A2) versus negative NVC (Condition A3). Figure 4c presents a significant difference between two groups (paired sample t test, $p < .001$).

3.5 | Linear and nonlinear interactions between neuronal and hemodynamic changes

To identify a linear relationship between EEG and NIRS data, changes in the RMS of the hemodynamic signals were plotted as a function of the RMS of the EEG. A slight linear correlation was found between the RMS of the bursts and the RMS of the hemodynamic responses (HbO, HbR, TOI, rCBF, and rCMRO$_2$; Figure 5a).

Transfer entropy analysis was used to identify a nonlinear and causal relationship between EEG and NIRS data, as it detects the relationship between the past of one signal and the present of another signal (Nourhashemi et al., 2017). Figure 5b shows the values of directionality = $(TE_{NIRS \to EEG}) - (TE_{EEG \to NIRS})$ for the 31 neonates, resulting in a fluctuating directionality between EEG and NIRS (DCS) with a tendency toward a negative directionality in 23/31 (21/31) preterm neonates and a positive directionality in the remaining 8 (10) preterm neonates. The negative values of directionality suggest that EEG was predominant over NIRS (DCS).

3.6 | The effect of age (wavelet real-time analysis of NVC in preterm neonates)

The percentage of significant coherence between the amplitude of the various hemodynamic parameter and the amplitude of the EEG burst were analyzed by wavelet coherence (Tian et al., 2016). Squared cross-wavelet coherence, $R^2_{rCBF \to EEG}$, reflected the overall degree at which rCBF and EEG were correlated at each timescale over the frequency range. Wavelet-based coherence was calculated in each preterm neonate, in the wavelet scale of 25–30 min equivalent to a very-low-frequency (VLF) range of 0.003–0.3 Hz (Figure 6b). The percentage of significant amplitude_coherence is shown in (Figure 6c) as a function of both time and frequency.

A positive correlation was observed between age and the percentage of significant coherence ($p < .05$) between the hemodynamic responses and EEG (rCBF-EEG, rCMRO$_2$-EEG, HbO-EEG, HbR-EEG, and TOI-EEG; $R^2 > .5$ in the frequency range of 0.003–0.3 Hz; Figure 6d).

3.7 | Assessment of the systemic impact as a potential confounder

As autoregulation is not fully mature in the newborn brain (Greisen, 2009), the dynamics and direction of the cortical hemodynamic response might be affected by stimulus-evoked increases in systemic blood pressure (Kozberg et al., 2013). To evaluate the possible contribution of blood pressure to the hemodynamic signal, accurate noninvasive beat-to-beat blood pressure monitoring was performed. Systemic blood pressure was not significantly correlated with the burst-evoked hemodynamic signal in the neonatal brain at rest (Figure 2, VIII and Figure 3, VIII), suggesting that the complexity of the observed NVC at rest was likely not related to systemic changes.

4 | DISCUSSION

This study highlights the complexity of coupling strategies between the immature neuronal and vascular networks in response to endogenous neuronal activation. More precisely, it shows that:

1. Spontaneous physiological neuronal bursts of activity in preterm infants (<35 weeks GA) at rest are coupled with various types of hemodynamic responses, such as (a) increases in rCBF and rCMRO$_2$ with no changes in rCBV with positive NVC, (b) decreases in rCBF, rCMRO$_2$, and rCBV with negative NVC, (c) increase/decrease in rCBV, rCMRO$_2$ with no changes in rCBF with either an increase or a decrease in HbO and HbR.
2. A developmental trajectory of the hemodynamic responses in the neonatal brain, which reflects the gradual development of NVC.
3. The various types of hemodynamic responses must be taken into account in order to more clearly characterize NVC to spontaneous bursts of activity in preterm infants.

4.1 | Cerebral hemodynamic patterns

Fine-tuning of neural wiring is subject to the maturation of inhibitory trajectories (Crook, Kisvarday, & Eysel, 1998). GABAergic interneurons, established at various stages after birth, are related to region-dependent critical periods (Le Magueresse & Monyer, 2013). In particular, there is a maturational shift from excitatory to inhibitory of the developing brain. This maturational transition occurs as a consequence of the change of the neurotransmitter GABA from depolarizing to hyperpolarizing at around Day 7 postpartum in mice (Amin & Marinaro, 2017). This shift has the potential to impact the profile of cerebral hemodynamics, as some studies have hypothesized that interneurons provide a crucial contribution to NVC (Cauli et al., 2004).

In addition, the weighting between arterial, venous, and capillary contributions to NVC is significantly different for excitatory and inhibitory tasks in the human brain (Huber et al., 2014). The interplay of the various vascular compartments in NVC, with their considerable prematurity (Miyawaki, Matsui, & Takashima, 1998), suggest different

hemodynamic patterns, resulting from different underlying hemodynamic mechanisms. The various patterns of hemodynamic response observed in this study could provide some explanation for the divergent hemodynamic responses previously reported in immature neurovascular networks and also suggest that the strategy developed to achieve NVC in preterm neonates is much more complex than in adults.

Data were firstly analyzed on the basis of burst activity, without taking into account the IBI or any putative hemodynamic response (positive or negative CBV or CBF changes), which could mask the complexity of the hemodynamic responses to the burst of activity that would be lost in averaging. NVC must be considered from different points of view in order to assess the variability of hemodynamic responses to similar bursts. One approach consists of analyzing the global hemodynamic response according to bursts alone (Subcondition A0). Another approach consists of considering the hemodynamic responses according to various types of bursts and particularly different IBI. The last approach consists of tracking the complexity of the response in terms of the hemodynamic response, by assuming that, instead of opposite changes in HbO and HbR resulting in a change in CBV, the hemodynamic response consists of similar changes in HbO and HbR resulting in a change of CBV only. This is an important point in view of the contradictory results concerning NVC in preterm infants. Many studies have described typical NVC in preterm infants. In particular, in our previous studies, we observed NVC in response to spontaneous activities in physiological and pathological situations (Roche-Labarbe et al., 2007) or external auditory stimulations (Mahmoudzadehet al., 2013). However, some studies did not observe typical NVC and many studies have reported negative NVC in response to exogenous stimulation (A. P. Born et al., 2000). Apart from the immaturity of intimate cellular mechanisms, these differences could also be due to the different strategies of the vascular system to respond to increased metabolic demand, depending on baseline status of the neuronal and hemodynamic system (Bourel-Ponchel, Mahmoudzadeh, Delignières, Berquin, & Wallois, 2017). According to the classification based on hemodynamic response, averaging of the various responses will obviously modify the global averaged hemodynamic output comprising a mix of positive and negative CBF or CBV responses, resulting in the absence of a hemodynamic response observed in Subcondition A0 without taking into account the IBI or the direction of HbO and HbR changes. Looking from the classification based on hemodynamic responses whatever the direction of CBF or CBV highlights this complexity and provides an explanation for the contradictory results concerning NVC in preterm infants.

4.2 | Positive hemodynamic response

The positive response most frequently observed confirms the ability of the vascular system to couple with neuronal activity in preterm neonates. These early hemodynamic changes, consisting of a significant initial decrease in HbO and increase in HbR prior to the onset of the EEG burst, together with a decrease in rCBF, likely corresponding to an increase in oxygen consumption, occurring before any EEG activities could be related to the hemodynamic consequences of a small number of synchronized activated neurons or activation of unsynchronized neurons during the first few seconds of activation (Roche-Labarbe et al., 2007). The origins of the burst recorded by EEG in preterm neonates remain unknown, but are likely to be related to intimate mechanisms between the developing subplate and the cortical plate with interplay between ascending pyramidal neurons and subplate neurons (Routier et al., 2017). Under these conditions, earlier endogenous activation of subplate neurons (Arichi et al., 2012), presenting an electromagnetic field that is not directed perpendicular to the surface of the brain, and which therefore cannot be detected by EEG recordings, may be able to develop NVC.

The typical pattern of NVC with its overflow, as described in adults (increase in HbO, decrease in HbR, and increase in rCBF and rCMRO$_2$), starts at the onset of the EEG burst, bringing oxygenated hemoglobin into the brain. The decreased HbR concentration during the burst further suggests that oxygen delivery exceeds oxygen consumption during spontaneous bursts in preterm neonates. This typical pattern suggests that all of the intimate cellular mechanisms that drive the two systems to coupling are already functional in immature neuronal and vascular networks and are sufficiently developed to produce the overflow with an increase in oxygen delivery that exceeds oxygen consumption, even under resting conditions.

The changes in HbO–HbR demonstrated by multidistance NIRS analysis support the idea that hemodynamic changes are the result of changes in the dynamics of cortical microvessels. The laser hemodynamic response supports pollution (or cross-talk) from deeper structures that progressively disappear from deep to superficial layers (Bourel-Ponchel et al., 2017).

When considering the hemodynamic response with an IBI of less than 20 s (Subconditions A2 and B2), the onset of a second burst was observed during the hemodynamic response of the previous burst, masking the initial decrease in HbO (increase in HBR) prior to the second burst, which was replaced by earlier onset of NVC in the presence of a short IBI. The subsequent pattern of hemodynamic changes remained similar regardless of these initial differences. Nevertheless, in view of the higher amplitude hemodynamic response observed with a short IBI, a cumulative effect likely occurred during NVC.

These typical patterns of NVC observed in preterm neonates further suggest that the various models developed to explain NVC in adults (Buxton, Uludag, Dubowitz, & Liu, 2004) and other models can be applied, to a certain extent, to immature neuronal and vascular networks very early in neurodevelopment from 28 weeks GA. In the positive NIRS response, an increased blood flow velocity not accompanied by either vasodilatation or recruitment might explain the absence of increase in HbT during activation, resulting in an increase in venous blood oxygenation.

4.3 | Negative NVC

Although typical NVC can be triggered by spontaneous endogenous activities, negative hemodynamic responses (decrease in HbO,

increase in HbR, decrease in rCBF and rCMRO$_2$ with no changes in CBV) were regularly observed regardless of the duration of the IBI. This type of negative coupling has been described in many experimental setups, not only in fNIRS, following peripheral stimulation (Maggioni et al., 2015), but also in fMRI [visual (A. P. Born et al., 2000; Martin et al., 1999; Sie et al., 2001), somatosensory (S. G. Erberich et al., 2006; Heep et al., 2009)]. The literature on the negative hemodynamic response remains controversial (M. T. Colonnese et al., 2007; Zimmermann et al., 2012). These negative hemodynamic responses have been attributed to a "negative surround" often characterized as either "vascular steal" or an index of reduced or inhibitory neural activity in adults (Boas, Jones, Devor, Huppert, & Dale, 2008). A steal effect from a neighboring cortical area is unlikely, as the whole brain presents the same type of activation during the bursts, as the bursts are likely to be generated by the subplate by means of a general mechanism such as coupling, mediated by Mayer–Traub–Hering hemodynamic waves or by means of an autonomic mechanism (Schwab, Groh, Schwab, & Witte, 2009; Witte et al., 2004). Alternatively, whole brain burst synchronization may be dependent on nonsynaptic events such as changes in pH, or [Ca^{++}] or drugs that interfere with the activity of connexin (Cx), known to modulate the time that SP neurons spend in an active state (Moore et al., 2009). In addition, hemodynamic measurements (CW-NIRS and FD-NIRS) recorded at a certain distance corroborate this hypothesis, as similar patterns of response were observed in areas that are not strictly identical.

Nevertheless, this negative hemodynamic response may also be an independent NVC potentially linked to cholinergic or noradrenergic-based vasoconstriction to regulate blood flow to activated regions (Bekar, Wei, & Nedergaard, 2012; Takata et al., 2013). However, this mechanism is not fully understood, whether this vasoconstriction restrict the degree of functional hemodynamic responses to preserve the frail neonatal vasculature, which predisposes to hemorrhage in preterm infants, as a result of excessive vasodilation and systemic hypertension (Volpe, 1997).

Alternatively, an inverted NVC related to a situation of anaerobic metabolism has been proposed to explain the hemodynamic response to epileptic spasms associated with metabolic dysfunction treated by a ketogenic diet only (Bourel-Ponchel et al., 2017). The negative NIRS seems to be driven by decreased CBF. A decrease in rCBF concomitant with a slight increase in HbR might reflect increasing oxygen extraction, as, due to limitations in oxygen transport, the brain switches to anaerobic glucose consumption during activation. Switching to anaerobic metabolism (Rodríguez-Balderrama, Ostia-Garza, Villarreal-Parra, & Tijerina-Guajardo, 2016) may be driven by the observed decrease in rCBF, rCMRO$_2$, and TOI, which could be explained by neonatal and early infantile maturation, corresponding to the period of rapid formation of synapses (Bourgeois, Jastreboff, & Rakic, 1989; Huttenlocher & Dabholkar, 1997).

4.4 | Volume changes

In addition to changes in rCBF, the neurovascular system also reacts to EEG bursts by changes in CBV with no associated changes in rCBF.

According to the various proposed models of NVC (Hoshi, Kobayashi, & Tamura, 2001), increases and decreases in blood volume with no changes in rCBF are more likely related to venous constriction and venous dilatation, respectively. Increases in both HbO and HbR with no change in rCBF support the hypothesis that O$_2$ consumption is not fully compensated by the increase in HbO, and the increased oxygen supply is therefore not sufficient to meet the increased oxygen demand. A similar pattern of hemodynamic response has also been observed in response to visual stimulation of neonates (Meek et al., 1998). Decreases in both HbO and HbR can be explained with the hypothesis that a decrease in HbO during a burst of activity is linked to an insufficient increase in rCBF, while a decrease in HbR reflects a decrease in venous blood oxygenation and blood volume (Hoshi et al., 2001).

The increased or decreased CBV could be related to the different contributions of various vascular compartments in NVC, as Huber et al. (2014) demonstrated that inhibitory stimuli are associated with decreased CBV (negative BOLD) due to constriction of surface arteries, while excitatory stimuli are accompanied by increased CBV (positive BOLD) in cortical and pial vasculature.

As a consequence of these three conditions, it can be concluded that, in positive NIRS conditions (Figure 2, A1 and A2 or Figure 3, B1 and B2), the magnitude of the decreases in HbR during the burst of activity can be attributed to venous hyperoxia due to overcompensation of blood flow. In negative NIRS conditions (Figure 2, A3 or Figure 3, B3), the increase in HbR mainly reflects venous hypoxia, whereas in volume change conditions (Figure 3, C1 and C2), changes in HbR mainly reflect changes in venous blood volume.

The various hemodynamic responses (comprising a significant number of positive NVC responses) observed reflect the complexity of the interactions between the neuronal and vascular networks in preterm neonates. A linear correlation was observed between the RMS of neuronal EEG activity and the RMS of the hemodynamic response, despite the possible implication of the subplate neurons and other nonsynchronized or poorly orientated pyramidal cells, which might participate in the elaboration of the type of neurovascular response triggered by the underlying neuronal activity (cortical plate or subplate). In addition, other nonoxidative metabolic mechanisms are likely to participate (Bourel-Ponchel et al., 2017). However, in a nonlinear investigation, the predominant driving influence of EEG on NIRS-DCS (or the inverse) differed in the various preterm neonates. Figure 5b is consistent with the leftward- and rightward-pointing arrow, which indicates flow of information in both directions. This phenomenon may have a multifactorial cause and could be related to regulation of brain hemodynamics (Caicedo et al., 2016).

4.5 | Assessment of NVC as a function of age by wavelet coherence analysis

The coupling between neuronal activation and the hemodynamic response (in the very low- frequency range 0.003–0.3 Hz) increased as a function of age, indicating progressive maturation of oscillatory

coupling of the neuronal and vascular networks. Slow rhythms in adults have also been shown to synchronize large spatial domains affecting various functions (71), and the findings of the present study tend to suggest age-related development of NVC. As the early post-partum brain appears to be very sensitive to stable cortical oxygenation, development of a timely functional hemodynamic response presumably constitutes an essential phase of development. Disconnection or delays in the onset of NVC could promote anomalies in both neural and vascular networks. As the multifaceted progress of neurovascular development prolongs occur after childbirth in natural development, attention to the potential contribution of this co-developing networks in normal and abnormal pathways of cerebral maturation was suggested for the future work. Although considering the age effect, different factors might impact the estimation of *absolute* HbO and HbR such as the head curvature (Dehaes et al., 2011), CSF and skull thicknesses. These putative errors are unlikely to impact drastically the dynamic of the relative changes in HbO and HbR in the current study (see Supporting Information for more details).

NVC depends not only on the IBI, but also on the characteristics of the burst activity (RMS), age and the hemodynamic status of the vascular network, as in cases of intraventricular hemorrhage (Lin, Hagan, Fenoglio, Grant, & Franceschini, 2016). Future studies must evaluate the impact of different metabolic states and different treatments in a larger cohort.

5 | CONCLUSION

The noninvasive functional hemodynamic imaging modalities (i.e., fMRI and fNIRS) used to investigate brain activity are based on assessment of hemodynamics as a proxy for neural activity. As NVC during early stages of brain maturation differs from that observed in adults, classical analysis and interpretation of functional hemodynamic data could be misleading. In contrast, with a better insight concerning interpretation of functional neuroimaging data in these populations, functional hemodynamic imaging approaches could be useful to describe the development of NVC.

This study describes the various pattern of cerebral hemodynamic response to spontaneous cerebral bursts of activity in the resting state in preterm neonates. The results should be interpreted in the context of the immature neuronal and vascular networks and the immature cellular mechanisms of NVC. The amplitude of spontaneous NVC at the resting state is described as being age-dependent.

In view of the immaturity of NVC, functional hemodynamic data obtained in preterm neonates, and probably term infants, need to be interpreted differently from adult data. This type of multimodal study paves the way for further research concerning which factors should be considered in the analysis of these data. We are confident that our results will improve our knowledge of neurovascular development. This multiscale, multimodal, noninvasive approach to NVC in spontaneous cerebral burst activity in preterm neonates allows investigation of the neuronal and vascular dimensions of NVC, corresponding to the same neurovascular functional system.

Altered neurovascular development is a factor involved in disorders of brain development, as neurovascular development is an essential element of neonatal brain development, together with neural development. A more detailed understanding of the normal development of NVC could give advance landscape of the etiology of neurodevelopmental disorders and may provide novel biomarkers for identification and analysis of therapeutic targets. In our view, these results represent an excellent initial step toward providing a unique approach to explore and assess this developmental process and to provide new therapeutic biomarkers. In future studies, NVC will be investigated in the group of preterm infants presenting various disorders such as patent ductus arteriosus (PDA) and intraventricular hemorrhage (IVH), under resting conditions.

CONFLICT OF INTEREST

The authors have indicated they have no financial relationships relevant to this article to disclose.

AUTHOR CONTRIBUTIONS

M.M., G.K., and F.W. designed the research; M.N., M.M. performed the research and analyzed data; S.G. and G.K. recruited patients and provided clinical support; and M.N., M.M., G.K., and F.W. wrote the paper. All authors discussed the results and implications and commented on the manuscript at all stages.

DATA AVAILABILITY STATEMENT

The data that support the findings of this study are available from the corresponding author upon reasonable request.

ORCID

Mahdi Mahmoudzadeh https://orcid.org/0000-0003-3145-2133
Fabrice Wallois https://orcid.org/0000-0003-2928-5428

REFERENCES

Ackman, J. B., Burbridge, T. J., & Crair, M. C. (2012). Retinal waves coordinate patterned activity throughout the developing visual system. *Nature, 490*(7419), 219–225. https://doi.org/10.1038/nature11529

Amin, H., & Marinaro, F. (2017). Developmental excitatory-to-inhibitory GABA-polarity switch is disrupted in 22q11.2 deletion syndrome: A potential target for clinical therapeutics. *Scientific Reports, 7*(1), 15752. https://doi.org/10.1038/s41598-017-15793-9

Arichi, T., Fagiolo, G., Varela, M., Melendez-Calderon, A., Allievi, A., Merchant, N., … Edwards, A. D. (2012). Development of BOLD signal

hemodynamic responses in the human brain. *NeuroImage*, *63*(2), 663–673. https://doi.org/10.1016/j.neuroimage.2012.06.054

Arichi, T., Moraux, A., Melendez, A., Doria, V., Groppo, M., Merchant, N., ... Edwards, A. D. (2010). Somatosensory cortical activation identified by functional MRI in preterm and term infants. *NeuroImage*, *49*(3), 2063–2071. https://doi.org/10.1016/j.neuroimage.2009.10.038

Attwell, D., & Iadecola, C. (2002). The neural basis of functional brain imaging signals. *Trends in Neurosciences*, *25*(12), 621–625.

Bekar, L. K., Wei, H. S., & Nedergaard, M. (2012). The locus coeruleus-norepinephrine network optimizes coupling of cerebral blood volume with oxygen demand. *Journal of Cerebral Blood Flow and Metabolism*, *32*(12), 2135–2145. https://doi.org/10.1038/jcbfm.2012.115

Boas, D. A., Jones, S. R., Devor, A., Huppert, T. J., & Dale, A. M. (2008). A vascular anatomical network model of the spatio-temporal response to brain activation. *NeuroImage*, *40*(3), 1116–1129. https://doi.org/10.1016/j.neuroimage.2007.12.061

Born, A. P., Miranda, M. J., Rostrup, E., Toft, P. B., Peitersen, B., Larsson, H. B., & Lou, H. C. (2000). Functional magnetic resonance imaging of the normal and abnormal visual system in early life. *Neuropediatrics*, *31*(1), 24–32. https://doi.org/10.1055/s-2000-15402

Born, P., Leth, H., Miranda, M. J., Rostrup, E., Stensgaard, A., Peitersen, B., ... Lou, H. C. (1998). Visual activation in infants and young children studied by functional magnetic resonance imaging. *Pediatric Research*, *44*(4), 578–583. https://doi.org/10.1203/00006450-199810000-00018

Bourel-Ponchel, E., Mahmoudzadeh, M., Delignières, A., Berquin, P., & Wallois, F. (2017). Non-invasive, multimodal analysis of cortical activity, blood volume and neurovascular coupling in infantile spasms using EEG-fNIRS monitoring. *NeuroImage: Clinical*, *15*, 359–366. https://doi.org/10.1016/j.nicl.2017.05.004

Bourgeois, J. P., Jastreboff, P. J., & Rakic, P. (1989). Synaptogenesis in visual cortex of normal and preterm monkeys: Evidence for intrinsic regulation of synaptic overproduction. *Proceedings of the National Academy of Sciences of the United States of America*, *86*(11), 4297–4301.

Buxton, R. B., Uludag, K., Dubowitz, D. J., & Liu, T. T. (2004). Modeling the hemodynamic response to brain activation. *NeuroImage*, *23*(Suppl 1), S220–S233. https://doi.org/10.1016/j.neuroimage.2004.07.013

Caicedo, A., Thewissen, L., Smits, A., Naulaers, G., Allegaert, K., & Van Huffel, S. (2016). Changes in oxygenation levels precede changes in amplitude of the EEG in premature infants. *Advances in Experimental Medicine and Biology*, *923*, 143–149. https://doi.org/10.1007/978-3-319-38810-6_19

Cauli, B., Tong, X. K., Rancillac, A., Serluca, N., Lambolez, B., Rossier, J., & Hamel, E. (2004). Cortical GABA interneurons in neurovascular coupling: Relays for subcortical vasoactive pathways. *The Journal of Neuroscience*, *24*(41), 8940–8949. https://doi.org/10.1523/JNEUROSCI.3065-04.2004

Chalia, M., Lee, C. W., Dempsey, L. A., Edwards, A. D., Singh, H., Michell, A. W., ... Cooper, R. J. (2016). Hemodynamic response to burst-suppressed and discontinuous electroencephalography activity in infants with hypoxic ischemic encephalopathy. *Neurophotonics*, *3*(3), 031408. https://doi.org/10.1117/1.NPh.3.3.031408

Colonnese, M. T., Phillips, M. A., Constantine-Paton, M., Kaila, K., & Jasanoff, A. (2007). Development of hemodynamic responses and functional connectivity in rat somatosensory cortex. *Nature Neuroscience*, *11*, 72–79.

Crook, J. M., Kisvarday, Z. F., & Eysel, U. T. (1998). Evidence for a contribution of lateral inhibition to orientation tuning and direction selectivity in cat visual cortex: Reversible inactivation of functionally characterized sites combined with neuroanatomical tracing techniques. *The European Journal of Neuroscience*, *10*(6), 2056–2075.

Dehaes, M., Grant, P. E., Sliva, D. D., Roche-Labarbe, N., Pienaar, R., Boas, D. A., ... Selb, J. (2011). Assessment of the frequency-domain multi-distance method to evaluate the brain optical properties: Monte Carlo simulations from neonate to adult. *Biomedical Optics Express*, *2*(3), 552–567. https://doi.org/10.1364/boe.2.000552

Erberich, G., Friedlich, P., & Seri, I. (2003). Brain activation detected by functional MRI in preterm neonates using an integrated radiofrequency neonatal head coil and MR compatible incubator. *NeuroImage*, *20*, 683–692.

Erberich, S. G., Panigrahy, A., Friedlich, P., Seri, I., Nelson, M. D., & Gilles, F. (2006). Somatosensory lateralization in the newborn brain. *NeuroImage*, *29*(1), 155–161. https://doi.org/10.1016/j.neuroimage.2005.07.024

Feller, M. B. (1999). Spontaneous correlated activity in developing neural circuits. *Neuron*, *22*(4), 653–656.

Gelfand, M. V., Hong, S., & Gu, C. (2009). Guidance from above: Common cues direct distinct signaling outcomes in vascular and neural patterning. *Trends in Cell Biology*, *19*(3), 99–110. https://doi.org/10.1016/j.tcb.2009.01.001

Greisen, G. (2009). To autoregulate or not to autoregulate—that is no longer the question. *Seminars in Pediatric Neurology*, *16*(4), 207–215. https://doi.org/10.1016/j.spen.2009.09.002

Greisen, G., Hellstrom-Vestas, L., Lou, H., Rosen, I., & Svenningsen, N. (1985). Sleep-waking shifts and cerebral blood flow in stable preterm infants. *Pediatric Research*, *19*(11), 1156–1159.

Grinsted, A., Moore, J. C., & Jevrejeva, S. (2004). Application of the cross wavelet transform and wavelet coherence to geophysical time series. *Nonlinear Processes in Geophysics*, *11*, 561–566.

Harris, J. J., Reynell, C., & Attwell, D. (2011). The physiology of developmental changes in BOLD functional imaging signals. *Developmental Cognitive Neuroscience*, *1*(3), 199–216. https://doi.org/10.1016/j.dcn.2011.04.001

Heep, A., Scheef, L., Jankowski, J., Born, M., Zimmermann, N., Sival, D., ... Boecker, H. (2009). Functional magnetic resonance imaging of the sensorimotor system in preterm infants. *Pediatrics*, *123*(1), 294–300. https://doi.org/10.1542/peds.2007-3475

Hoshi, Y., Kobayashi, N., & Tamura, M. (2001). Interpretation of near-infrared spectroscopy signals: A study with a newly developed perfused rat brain model. *Journal of Applied Physiology (Bethesda, MD: 1985)*, *90*(5), 1657–1662. https://doi.org/10.1152/jappl.2001.90.5.1657

Huber, L., Goense, J., Kennerley, A. J., Ivanov, D., Krieger, S. N., Lepsien, J., ... Moller, H. E. (2014). Investigation of the neurovascular coupling in positive and negative BOLD responses in human brain at 7 T. *NeuroImage*, *97*, 349–362. https://doi.org/10.1016/j.neuroimage.2014.04.022

Huttenlocher, P. R., & Dabholkar, A. S. (1997). Regional differences in synaptogenesis in human cerebral cortex. *The Journal of Comparative Neurology*, *387*(2), 167–178.

Huttenlocher, P. R., de Courten, C., Garey, L. J., & Van der Loos, H. (1982). Synaptogenesis in human visual cortex—evidence for synapse elimination during normal development. *Neuroscience Letters*, *33*(3), 247–252.

Iadecola, C., Li, J., Xu, S., & Yang, G. (1996). Neural mechanisms of blood flow regulation during synaptic activity in cerebellar cortex. *Journal of Neurophysiology*, *75*(2), 940–950. https://doi.org/10.1152/jn.1996.75.2.940

Jobsis, F. F. (1977). Noninvasive, infrared monitoring of cerebral and myocardial oxygen sufficiency and circulatory parameters. *Science*, *198*(4323), 1264–1267.

Kozberg, M., & Hillman, E. (2016). Neurovascular coupling and energy metabolism in the developing brain. *Progress in Brain Research*, *225*, 213–242. https://doi.org/10.1016/bs.pbr.2016.02.002

Kozberg, M. G., Chen, B. R., DeLeo, S. E., Bouchard, M. B., & Hillman, E. M. (2013). Resolving the transition from negative to positive blood oxygen level-dependent responses in the developing brain. *Proceedings of the National Academy of Sciences of the United States of America*, *110*(11), 4380–4385. https://doi.org/10.1073/pnas.1212785110

Le Magueresse, C., & Monyer, H. (2013). GABAergic interneurons shape the functional maturation of the cortex. *Neuron*, *77*(3), 388–405. https://doi.org/10.1016/j.neuron.2013.01.011

Lewis, T. L., Jr., Courchet, J., & Polleux, F. (2013). Cell biology in neuroscience: Cellular and molecular mechanisms underlying axon formation, growth, and branching. *The Journal of Cell Biology*, *202*(6), 837–848. https://doi.org/10.1083/jcb.201305098

Lin, P.-Y., Hagan, K., Fenoglio, A., Grant, P. E., & Franceschini, M. A. (2016). Reduced cerebral blood flow and oxygen metabolism in extremely preterm neonates with low-grade germinal matrix-intraventricular hemorrhage. *Scientific Reports*, 6, 25903–25903. https://doi.org/10.1038/srep25903

Maggioni, E., Molteni, E., Zucca, C., Reni, G., Cerutti, S., Triulzi, F. M., … Bianchi, A. M. (2015). Investigation of negative BOLD responses in human brain through NIRS technique. A visual stimulation study. *NeuroImage*, 108, 410–422. https://doi.org/10.1016/j.neuroimage.2014.12.074

Mahmoudzadeh, M., Dehaene-Lambertz, G., Fournier, M., Kongolo, G., Goudjil, S., Dubois, J., … Wallois, F. (2013). Syllabic discrimination in premature human infants prior to complete formation of cortical layers. *Proceedings of the National Academy of Sciences of the United States of America*, 110 (12), 4846–4851. https://doi.org/10.1073/pnas.1212220110

Mahmoudzadeh, M., Dehaene-Lambertz, G., & Wallois, F. (2017). Electrophysiological and hemodynamic mismatch responses in rats listening to human speech syllables. *PLoS One*, 12(3), e0173801. https://doi.org/10.1371/journal.pone.0173801

Maraun, D., & Kurths, J. (2004). Cross wavelet analysis: Significance testing and pitfalls. *Nonlinear Processes in Geophysics*, 11(4), 505–514.

Marin-Padilla, M. (1983). Structural organization of the human cerebral cortex prior to the appearance of the cortical plate. *Anatomy and Embryology (Berlin)*, 168(1), 21–40.

Martin, E., Joeri, P., Loenneker, T., Ekatodramis, D., Vitacco, D., Hennig, J., & Marcar, V. L. (1999). Visual processing in infants and children studied using functional MRI. *Pediatric Research*, 46(2), 135–140.

Meek, J. H., Firbank, M., Elwell, C. E., Atkinson, J., Braddick, O., & Wyatt, J. S. (1998). Regional hemodynamic responses to visual stimulation in awake infants. *Pediatric Research*, 43(6), 840–843. https://doi.org/10.1203/00006450-199806000-00019

Milligan, D. W. A. (1979). Cerebral blood flow and sleep state in the normal newborn infant. *Early Human Development*, 3(4), 321–328. https://doi.org/10.1016/0378-3782(79)90043-4

Miyawaki, T., Matsui, K., & Takashima, S. (1998). Developmental characteristics of vessel density in the human fetal and infant brains. *Early Human Development*, 53(1), 65–72.

Moore, A. R., Filipovic, R., Mo, Z., Rasband, M. N., Zecevic, N., & Antic, S. D. (2009). Electrical excitability of early neurons in the human cerebral cortex during the second trimester of gestation. *Cerebral Cortex*, 19(8), 1795–1805. https://doi.org/10.1093/cercor/bhn206

Mukhtar, A. I., Cowan, F. M., & Stothers, J. K. (1982). Cranial blood flow and blood pressure changes during sleep in the human neonate. *Early Human Development*, 6(1), 59–64. https://doi.org/10.1016/0378-3782(82)90057-3

Nelle, M., Hoecker, C., & Linderkamp, O. (1997). Effects of bolus tube feeding on cerebral blood flow velocity in neonates. *Archives of Disease in Childhood. Fetal and Neonatal Edition*, 76(1), F54–F56.

Nourhashemi, M., Kongolo, G., Mahmoudzadeh, M., Goudjil, S., & Wallois, F. (2017). Relationship between relative cerebral blood flow, relative cerebral blood volume, and relative cerebral metabolic rate of oxygen in the preterm neonatal brain. *Neurophotonics*, 4(2), 021104. https://doi.org/10.1117/1.NPh.4.2.021104

Roche-Labarbe, N., Wallois, F., Ponchel, E., Kongolo, G., & Grebe, R. (2007). Coupled oxygenation oscillation measured by NIRS and intermittent cerebral activation on EEG in premature infants. *NeuroImage*, 36(3), 718–727. https://doi.org/10.1016/j.neuroimage.2007.04.002

Rodríguez-Balderrama, I., Ostia-Garza, P. J., Villarreal-Parra, R. D., & Tijerina-Guajardo, M. (2016). Risk factors and the relation of lactic acid to neonatal mortality in the first week of life. *Medicina Universitaria*, 18 (70), 3–9. https://doi.org/10.1016/j.rmu.2015.12.001

Routier, L., Mahmoudzadeh, M., Panzani, M., Azizollahi, H., Goudjil, S., Kongolo, G., & Wallois, F. (2017). Plasticity of neonatal neuronal networks in very premature infants: Source localization of temporal theta activity, the first endogenous neural biomarker, in temporoparietal areas. *Human Brain Mapping*, 38(5), 2345–2358. https://doi.org/10.1002/hbm.23521

Schwab, K., Groh, T., Schwab, M., & Witte, H. (2009). Nonlinear analysis and modeling of cortical activation and deactivation patterns in the immature fetal electrocorticogram. *Chaos*, 19(1), 015111. https://doi.org/10.1063/1.3100546

Shannon, C. E. (1948). A mathematical theory of communication. *Bell System Technical Journal*, 27(3), 379–423. https://doi.org/10.1002/j.1538-7305.1948.tb01338.x

Sheth, S. A., Nemoto, M., Guiou, M., Walker, M., Pouratian, N., & Toga, A. W. (2004). Linear and nonlinear relationships between neuronal activity, oxygen metabolism, and hemodynamic responses. *Neuron*, 42(2), 347–355.

Sie, L. T. L., Rombouts, S. A., Valk, I. J., Hart, A. A., Scheltens, P., & van der Knaap, M. S. (2001). Functional MRI of visual cortex in sedated 18 month-old infants with or without periventricular leukomalacia. *Developmental Medicine and Child Neurology*, 43(7), 486–490.

Takata, N., Nagai, T., Ozawa, K., Oe, Y., Mikoshiba, K., & Hirase, H. (2013). Cerebral blood flow modulation by basal forebrain or whisker stimulation can occur independently of large cytosolic Ca2+ signaling in astrocytes. *PLoS One*, 8(6), e66525. https://doi.org/10.1371/journal.pone.0066525

Tian, F., Tarumi, T., Liu, H., Zhang, R., & Chalak, L. (2016). Wavelet coherence analysis of dynamic cerebral autoregulation in neonatal hypoxic–ischemic encephalopathy. *NeuroImage: Clinical*, 11, 124–132. https://doi.org/10.1016/j.nicl.2016.01.020

Vanhatalo, S., Palva, J. M., Andersson, S., Rivera, C., Voipio, J., & Kaila, K. (2005). Slow endogenous activity transients and developmental expression of K+-Cl− cotransporter 2 in the immature human cortex. *The European Journal of Neuroscience*, 22(11), 2799–2804. https://doi.org/10.1111/j.1460-9568.2005.04459.x

Volpe, J. J. (1997). Brain injury in the premature infant – From pathogenesis to prevention. *Brain and Development*, 19(8), 519–534. https://doi.org/10.1016/S0387-7604(97)00078-8

Wallois, F. (2010). Synopsis of maturation of specific features in EEG of premature neonates. *Neurophysiologie Clinique*, 40(2), 125–126. https://doi.org/10.1016/j.neucli.2010.02.001

Wang, D. B., Blocher, N. C., Spence, M. E., Rovainen, C. M., & Woolsey, T. A. (1992). Development and remodeling of cerebral blood vessels and their flow in postnatal mice observed with in vivo videomicroscopy. *Journal of Cerebral Blood Flow and Metabolism*, 12(6), 935–946. https://doi.org/10.1038/jcbfm.1992.130

Witte, H., Putsche, P., Schwab, K., Eiselt, M., Helbig, M., & Suesse, T. (2004). On the spatio-temporal organisation of quadratic phase-couplings in 'trace alternant' EEG pattern in full-term newborns. *Clinical Neurophysiology*, 115(10), 2308–2315. https://doi.org/10.1016/j.clinph.2004.05.014

Zimmermann, B. B., Roche-Labarbe, N., Surova, A., Boas, D. A., Wolf, M., Grant, P. E., & Franceschini, M. A. (2012). The confounding effect of systemic physiology on the hemodynamic response in newborns. *Advances in Experimental Medicine and Biology*, 737, 103–109. https://doi.org/10.1007/978-1-4614-1566-4_16

SUPPORTING INFORMATION

Additional supporting information may be found online in the Supporting Information section at the end of this article.